

Cluster mass functions in the quintessential Universe

Ewa L. Łokas¹, Paul Bode² and Yehuda Hoffman³

¹*Nicolaus Copernicus Astronomical Center, Bartycka 18, 00-716 Warsaw, Poland*

²*Princeton University Observatory, Princeton, NJ 08544-1001, USA*

³*Racah Institute of Physics, Hebrew University, Jerusalem 91904, Israel*

7 February 2020

ABSTRACT

We use N -body simulations to measure mass functions in flat cosmological models with quintessence characterized by constant w with $w = -1, -2/3$ and $-1/2$. The results are compared to the predictions of the formula proposed by Jenkins et al. at different redshifts, in terms of FOF masses as well as Abell masses appropriate for direct comparison to observations. The formula reproduces quite well the mass functions of simulated haloes in models with quintessence. We use the cluster mass function data at a number of redshifts from Carlberg et al. to constrain Ω_0 , σ_8 and w . The best fit is obtained in the limit $w \rightarrow 0$, but none of the values of w in the considered range $-1 \leq w < 0$ can actually be excluded. However, the adopted value of w affects significantly the constraints in the $\Omega_0 - \sigma_8$ plane. Taking into account the dependence on w we find $\Omega_0 = 0.32 \pm 0.15$ and $\sigma_8 = 0.85^{+0.38}_{-0.12}$ (68% c.l.). Since less negative w push the confidence regions toward higher Ω_0 and lower σ_8 we conclude that relaxing the assumption of $w = -1$ typically made in such comparisons may resolve the discrepancy between recent cluster mass function results (yielding rather low Ω_0 and high σ_8) and most other estimates.

Key words: methods: N -body simulations – methods: analytical – cosmology: theory – cosmology: dark matter – galaxies: clusters: general – large-scale structure of Universe

1 INTRODUCTION

Recently, our knowledge on background cosmology has improved dramatically due to new supernovae and cosmic microwave background data. Current observations favor a flat Universe with $\Omega_0 \approx 0.3$ (see e.g. Harun-or-Rashid & Roos 2001; Krauss 2003 and references therein) and the remaining contribution in the form of cosmological constant or some other form of dark energy. A class of models that satisfy these observational constraints has been proposed by Caldwell, Dave, & Steinhardt (1998) where the cosmological constant is replaced with an energy component characterized by the equation of state $p/\varrho = w \neq -1$. The component can cluster on largest scales and therefore affect the mass power spectrum (Ma et al. 1999) and microwave background anisotropies (Doran et al. 2001; Balbi et al. 2001; Caldwell & Doran 2003; Caldwell et al. 2003).

A considerable effort has gone into attempts to put constraints on models with quintessence and presently the values of $-1 < w < -0.6$ seem most feasible observationally (Wang et al. 2000; Huterer & Turner 2001; Jimenez 2003). Another direction of investigations is into the physical basis for the existence of such component with the oldest attempts going back to Ratra & Peebles (1988). One of the

promising models is based on so-called “tracker fields” that display an attractor-like behaviour causing the energy density of quintessence to follow the radiation density in the radiation dominated era, but dominate over matter density after matter-radiation equality (Zlatev, Wang, & Steinhardt 1999; Steinhardt, Wang, & Zlatev 1999). It is still debated, however, how w should depend on time, and whether its redshift dependence can be reliably determined observationally (Barger & Marfatia 2001; Maor, Brustein, & Steinhardt 2001; Weller & Albrecht 2001; Jimenez 2003; Majumdar & Mohr 2003).

From the gravitational instability point of view, the quintessence field and the cosmological constant play a very similar role: both can be treated as (unclustered) dark energy components that differ by their equation of state parameter, w . Technically, the equations governing the expansion of the Universe and the growth of density perturbations in the two models differ only by the value of w . Given the growing popularity of models with quintessence, in this paper we generalize the description of the mass functions to include its effect.

The mass function of clusters of galaxies has been used extensively to estimate cosmological parameters, especially Ω_0 and the rms density fluctuation σ_8 , usually yielding (due

to degeneracy) a constraint on some combination of the two. It has been shown that this degeneracy can be significantly decreased by using the data at different redshifts (Carlberg et al. 1997a; Bahcall, Fan & Cen 1997; Bahcall & Bode 2003) due to different growth rates of density fluctuations in different models. The growth rate also varies among models with different w ; one may therefore hope to distinguish between them by analyzing mass function data at high redshift. It is worth noting that the power spectra of models differing only by w are different only at very large scales, so the rms density fluctuations at scales of interest are almost identical when normalized to σ_8 .

The paper is organized as follows. In Section 2 we briefly summarize the properties of the cosmological model with quintessence, including the linear growth factor of density fluctuations. Section 3 presents the N -body simulations and the mass function measured from their output. In Section 4 we describe the transformation between mass functions in terms of FOF masses and in terms of Abell masses. Section 5 is devoted to the comparison of the theoretical mass functions to the data for clusters at different redshifts to obtain constraints on cosmological parameters. The Discussion follows in Section 6.

2 THE COSMOLOGICAL MODEL

Quintessence obeys the following equation of state relating its density ϱ_Q and pressure p_Q

$$p_Q = w\varrho_Q, \quad \text{where } -1 \leq w < 0. \quad (1)$$

The case of $w = -1$ corresponds to the usually defined cosmological constant.

The evolution of the scale factor $a = R/R_0 = 1/(1+z)$ (normalized to unity at present) in the quintessential Universe is governed by the Friedmann equation

$$\frac{da}{dt} = \frac{H_0}{f(a)}, \quad (2)$$

where

$$f(a) = \left[1 + \Omega_0 \left(\frac{1}{a} - 1 \right) + q_0 \left(\frac{1}{a^{1+3w}} - 1 \right) \right]^{-1/2} \quad (3)$$

and H_0 is the present value of the Hubble parameter. The quantities with subscript 0 here and below denote the present values. The parameter Ω is the standard measure of the amount of matter in units of critical density and q measures the density of quintessence in the same units:

$$q = \frac{\varrho_Q}{\varrho_{\text{crit}}}. \quad (4)$$

The Einstein equation for acceleration $d^2a/dt^2 = -4\pi G a(p + \varrho/3)$ shows that $w < -1/3$ is needed for the accelerated expansion to occur.

Solving the equation for the conservation of energy $d(\varrho_Q a^3)/da = -3p_Q a^2$ with condition (1), we get the following evolution of the density of quintessence in the general case of $w = w(a)$:

$$\varrho_Q = \varrho_{Q,0} \exp \left[-3 \ln a + 3 \int_a^1 \frac{w(a)da}{a} \right] \quad (5)$$

in agreement with Caldwell et al. (1998). For $w = \text{const}$, the case considered in this paper, the formula reduces to

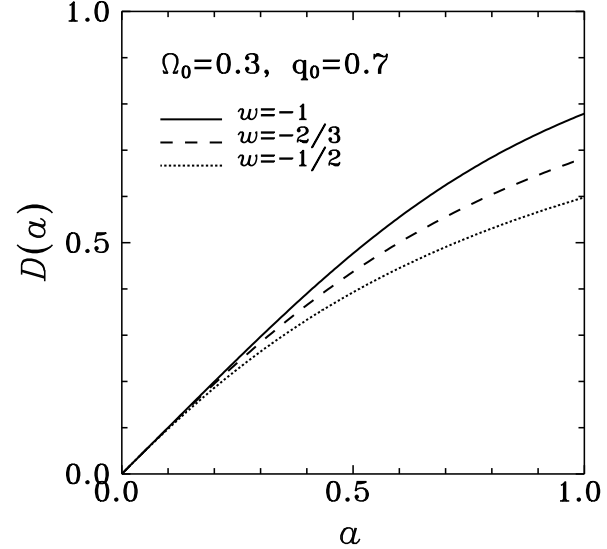


Figure 1. The linear growth rate of density fluctuations for $\Omega_0 = 0.3$, $q_0 = 0.7$ in three cases of $w = -1, -2/3$ and $-1/2$.

$$\varrho_Q = \varrho_{Q,0} a^{-3(1+w)}. \quad (6)$$

The evolution of Ω and q with scale factor (or equivalently redshift) is given by

$$\Omega(a) = \frac{\Omega_0 f^2(a)}{a}, \quad (7)$$

$$q(a) = \frac{q_0 f^2(a)}{a^{1+3w}} \quad (8)$$

while the Hubble parameter itself evolves so that $H(a) = H_0/[a f(a)]$.

The linear evolution of the matter density contrast $\delta = \delta\varrho/\varrho$ is governed by equation $\ddot{\delta} + 2(\dot{a}/a)\dot{\delta} - 4\pi G\varrho\delta = 0$, where dots represent derivatives with respect to time. For flat models and arbitrary w an analytical expression for $D(a)$ was found by Silveira & Waga (1994, corrected for typos). With our notation and the normalization of $D(a) = a$ for $\Omega = 1$ and $q = 0$, it becomes

$$D(a) = a {}_2F_1 \left[-\frac{1}{3w}, \frac{w-1}{2w}, 1 - \frac{5}{6w}, -a^{-3w} \frac{1-\Omega_0}{\Omega_0} \right] \quad (9)$$

where ${}_2F_1$ is a hypergeometric function. The solutions (9) for $w = -1, -2/3$ and $-1/2$ are plotted in Figure 1 for the cosmological parameters $\Omega_0 = 0.3$ and $q_0 = 0.7$.

3 THE SIMULATED MASS FUNCTIONS

In order to study the cluster mass functions in models with quintessence we have used a subset of the Gpc^3 dark matter N -body simulations of Bode et al. (2001). Among the family of cosmological models they considered two are of interest for us here: ΛCDM (with $w = -1$, $\Omega_0 = 0.3$, $q_0 = 0.7$, $\Omega_b = 0.04$, $h = 0.67$, $\sigma_8 = 0.9$) and QCDM (with $w = -2/3$, $\sigma_8 = 0.84$, and all other parameters the same). Both models had the primordial spectral index $n = 1$. The $w = -1$ and $w = -2/3$ simulations were carried out using the Tree-Particle-Mesh (TPM) code described in Bode, Ostriker & Xu (2000).

For the purpose of this study, a new simulation with $w = -1/2$ (and $\sigma_8 = 0.88$, with all the remaining parameters unchanged) was run using a newer, publically available version of TPM code which includes a number of improvements over the earlier code (Bode & Ostriker 2003). The changes in the code which would affect the numerical results include improvements in the time stepping (adding individual particle time steps within trees, and a stricter time step criterion) and domain decomposition (adding an improved treatment of tidal forces, and a new selection criterion for regions of full force resolution). The changes in time step only affect the innermost cores of collapsed objects, where the relaxation time is short (Bode & Ostriker 2003), leaving the mass function unchanged. The changes in domain decomposition affect the mass function, but only at the low-mass end: in the $w = -1$ and $w = -2/3$ simulations, the mass function is complete only above $6 \times 10^{13} h^{-1} M_\odot$ (100 particles), while in the $w = -1/2$ run it extends down to $10^{13} h^{-1} M_\odot$ (16 particles). In this paper we concentrate on the high-mass end of the mass function, where these numerical differences have no impact.

The identification of halos in the final particle distribution has been performed with the standard friends-of-friends (FOF) halo-finding algorithm with the linking parameter $b = 0.2$ (particles are linked if their separation is smaller than b times mean interparticle distance). As an alternative, we have also used the HOP regrouping algorithm (Eisenstein & Hut 1998). This procedure employs several parameters; however, the resulting mass function is sensitive to only one of them, the density (in units of the background density) at the outer boundary of the halo, δ_{outer} . As discussed by Eisenstein & Hut (1998), assuming $\delta_{\text{outer}} = 80$ is equivalent to using the linking parameter of $b = 0.2$ in the FOF halo-finding algorithm. Indeed, we verified that the mass functions measured in the simulations are almost identical when using these two halo-finding schemes.

Figure 2 shows in solid lines the mass functions measured with FOF from N -body simulations with $w = -1$ (upper panel), $w = -2/3$ (middle panel) and $w = -1/2$ (lower panel) at redshifts $z = 0, 0.5, 1$ and 2 . The quantity plotted is the cumulative mass function (the comoving number density of objects of mass greater than M) $N(> M) = \int_M^\infty n(M) dM$, where $n(M)$ is the number density of objects with mass between M and $M + dM$. Jenkins et al. (2001) established that when the masses are identified with FOF(0.2) the simulated mass function in different cosmologies and at different epochs can be well approximated by the following fitting formula

$$n_J(M) = -\frac{\varrho_b}{\sigma M} \frac{d\sigma}{dM} F(M) \quad (10)$$

where

$$F(M) = 0.315 \exp(-|\ln \sigma^{-1} + 0.61|^{3.8}). \quad (11)$$

In the above formulae ϱ_b is the background density, σ is the rms density fluctuation at top-hat smoothing scale R

$$\sigma^2 = \frac{D^2(a)}{(2\pi)^3} \int d^3k P(k) W_{\text{TH}}^2(kR) \quad (12)$$

where $D(a)$ is the linear growth factor given by equation (9), $W_{\text{TH}}(kR)$ is the top-hat filter in Fourier space and the mass is related to the smoothing scale by $M = 4\pi\varrho_b R^3/3$.

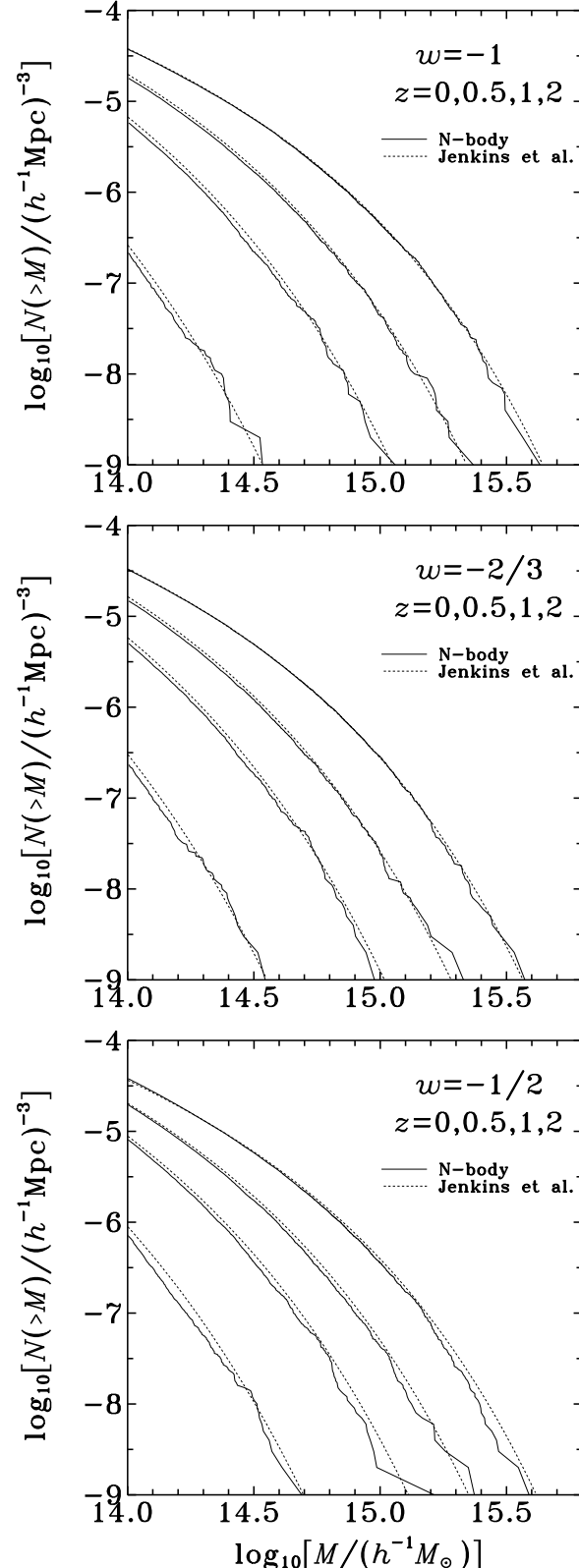


Figure 2. Comparison of the N -body cumulative mass functions (solid lines) obtained with $w = -1$ (upper panel), $w = -2/3$ (middle panel) and $w = -1/2$ (lower panel) to the predictions of the Jenkins formula (dotted lines) at different redshifts $z = 0, 0.5, 1$ and 2 .

$P(k)$ in equation (12) is the power spectrum of density fluctuations, which we assume here to be given in the form proposed by Ma et al. (1999) for flat models. For the present time ($a = 1$) the power spectrum is $P(k) = Ck^n T^2(k)$ where n is the primordial power spectrum index (we will assume $n = 1$) and $T(k)$ is the transfer function. For the case of cosmological constant (Λ CDM) we take the transfer function T_Λ in the form proposed by Sugiyama (1995)

$$T_\Lambda^2(p) = \frac{\ln^2(1 + 2.34p)}{(2.34p)^2} \times [1 + 3.89p + (16.1p)^2 + (5.46p)^3 + (6.71p)^4]^{-1/2} \quad (13)$$

where $p = k/(\Gamma h \text{Mpc}^{-1})$ and $\Gamma = \Omega_0 h \exp[-\Omega_b(1 + \sqrt{2h}/\Omega_0)]$.

For models with quintessence the transfer function is $T_Q = T_{Q\Lambda} T_\Lambda$, where $T_{Q\Lambda} = T_Q/T_\Lambda$ can be approximated by fits given in Ma et al. (1999). However, for $w \neq -1$, $T_{Q\Lambda}$ differs from unity only at very large scales, i.e. very small wavenumbers. Thus if the spectra are normalized to σ_8 (the rms density fluctuation smoothed with $R = 8h^{-1}$ Mpc), then there is no need to introduce the correction from T_Λ to T_Q in (12) because it does not affect the calculation of σ .

The predictions for $N(> M)$ obtained from equations (10)-(13) for different w and redshifts are shown in Figure 2 as dotted lines. One can see that the Jenkins formula accurately reproduces the simulated mass function (with small discrepancies at higher redshifts) and therefore, although originally designed on basis of other cosmological models, it can be considered valid also in the presence of quintessence. We therefore confirm the result of Linder & Jenkins (2003) who also found a good agreement between the simulations and the predictions of Jenkins et al. (2001) formula in a different quintessence model.

4 FROM FOF TO VIRIAL AND ABELL MASSES

The masses of clusters of galaxies are usually measured as the so-called Abell masses, i.e. the masses inside the Abell radii of $1.5h^{-1}$ Mpc. For the purpose of comparison with observations we need to transform the mass functions expressed in terms of the FOF masses to Abell masses. This can be done assuming a density distribution inside the cluster. Since clusters are believed to be dominated by dark matter (e.g. Carlberg et al. 1997b; Biviano & Girardi 2003; Lokas & Mamon 2003) their density distribution can be well approximated by the universal profile proposed by Navarro, Frenk & White (1997, NFW) for dark matter haloes

$$\frac{\rho(s)}{\rho_b(z)} = \frac{\Delta_c c^2 g(c)}{3\Omega(z)s(1+cs)^2} \quad (14)$$

where the radius has been expressed in units of the virial radius r_v , $s = r/r_v$. The virial radius is defined as the distance from the centre of the halo within which the mean density is Δ_c times the critical density, ρ_{crit} . The value of the virial overdensity Δ_c is estimated from the spherical collapse model and depends on the cosmological model. For flat models with constant quintessence parameter w , its behaviour can be well approximated as (Weinberg & Kamionkowski 2003)

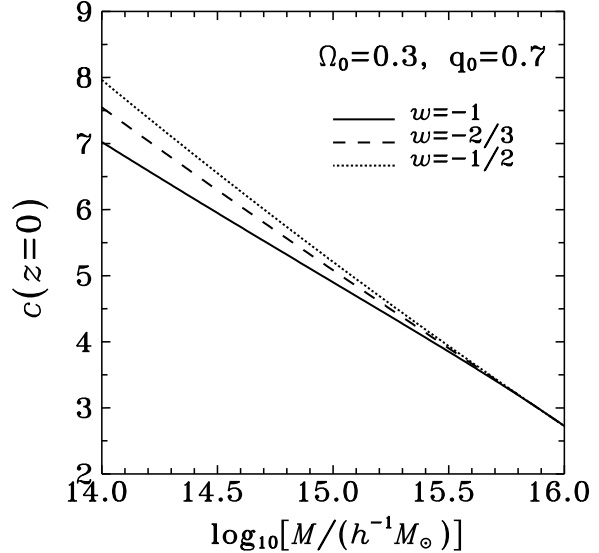


Figure 3. The concentration parameter at $z = 0$ calculated from the model of Bullock et al. for $\Omega_0 = 0.3$, $q_0 = 0.7$ and $w = -1, -2/3$ and $-1/2$ with the remaining parameters as in the simulations, except that we kept $\sigma_8 = 0.9$ for all cases.

$$\Delta_c = 18\pi^2(1 + a\theta^b)\Omega(z) \quad (15)$$

with $\theta = (1/\Omega_0 - 1)(1 + z)^{3w}$ and $a = 0.399 - 1.309[(-w)^{0.426} - 1]$, $b = 0.941 - 0.205[(-w)^{0.938} - 1]$.

The quantity c introduced in equation (14) is the concentration parameter, $c = r_v/r_s$, where r_s is the scale radius (at which the slope of the profile is r^{-2}). The function $g(c)$ in equation (14) is $g(c) = 1/[\ln(1 + c) - c/(1 + c)]$. From cosmological N -body simulations (NFW; Jing 2000; Jing & Suto 2000; Bullock et al. 2001), we know that c depends on the mass and redshift of formation of the object, as well as the initial power spectrum of density fluctuations. We will approximate this dependence using the toy model of Bullock et al. (2001) (their equations (9)-(13) with parameters $F = 0.001$ and $K = 3.0$ as advertised for masses $M > 10^{14}h^{-1}M_\odot$). The predictions of the model at $z = 0$ for cosmological models as in our simulations (but all normalized to $\sigma_8 = 0.9$) is shown in Figure 3 for masses $10^{14} - 10^{16}h^{-1}M_\odot$. For higher redshifts we assume $c(z) = c(z = 0)/(1 + z)$, following Bullock et al. (2001). The dependence of the concentration on w is rather weak but there is a trend of larger c values for less negative w . A similar trend was observed in the properties of dark haloes obtained in the N -body simulations by Klypin et al. (2003), although for smaller masses.

Since the NFW profile describes the halo properties in terms of the virial radius and the corresponding virial mass $M_v = 4\pi r_v^3 \Delta_c \rho_{\text{crit}}/3$, we have to transform the FOF masses first to virial masses. As previously noted, the FOF parameter $b = 0.2$ corresponds to the local overdensity at the border of the halo $\delta_{\text{outer}} = 80$. Therefore we will assume that the FOF masses are equal to masses enclosed by such isodensity contour, $M_{\text{FOF}} = M_{80}$. Using the NFW distribution we find that for our simulated Λ CDM model at $z = 0$ we have $M_{80} \approx M_v$, while for higher redshifts $M_{80} < M_v$. In the case of models with $w = -2/3$ we instead get $M_{80} > M_v$,

and more so for $w = -1/2$. The differences between M_{80} and M_v for the models, redshifts and mass range considered here are typically of the order of a few percent and do not exceed 20%. They depend somewhat on mass, and are due mainly to the dependence of Δ_c on cosmology. Once the FOF masses are translated to virial masses we can obtain the Abell masses M_A using the NFW mass distribution following from equation (14)

$$M_A = M(s_A) = M_v g(c) \left[\ln(1 + cs_A) - \frac{cs_A}{1 + cs_A} \right] \quad (16)$$

where $s_A = r_A/r_v$ is the Abell radius in units of the virial radius.

Figure 4 shows the cumulative mass functions in terms of the Abell masses as measured in the simulations (solid lines) and as calculated with the Jenkins formula (10)-(11) with the proper mass transformation (dotted lines). The agreement is very good for $z = 0$. In general, the analytic predictions match the N -body results as long as the virial radius is near or greater than the Abell radius. However, at higher redshifts the predictions for lower masses are overestimated. Several effects might lead to this disagreement. Abell masses were measured in the simulations in the manner described in Bode et al. (2001). In this method, clusters cannot be closer together than $1 h^{-1} \text{Mpc}$; also, if two Abell radii overlap, particles in the overlap region are only included in one of the clusters (based on binding energy). These two factors may lead to fewer objects – lower mass objects being subsumed into larger ones.

As discussed by Bode et al. (2001) higher resolution simulations produce somewhat steeper Abell mass functions which would agree better with the predictions. We must also keep in mind that the result was obtained with the assumption of NFW profile, while for smaller haloes this may not be the case. The haloes of mass $10^{14} h^{-1} M_\odot$ have only 160 particles in our simulations and can hardly be expected to have a well defined density profile. We have also extrapolated the model for concentration of Bullock et al. (2001) both for quintessence and very large masses, two regimes where it has never been tested, while even in well studied models concentration shows substantial scatter. Given the number of approximations involved in the result we conclude that the fits are satisfactory, especially in the mass range between the two vertical dashed lines in each panel of Figure 4, covered by the data, which will be used in the next Section.

5 COMPARISON WITH OBSERVATIONS

For comparison of the theoretical mass functions with observations we used the data for cluster mass function from Carlberg et al. (1997a). The data consist of seven data points of $N(> M)$ for different Abell masses $M > 4 \times 10^{14} h^{-1} M_\odot$, for redshift bins in the range $0 < z < 0.85$. There are four data points coming from different surveys in the low redshift bin $0 < z < 0.1$ and three data points in higher redshift bins $0.18 < z < 0.35$, $0.35 < z < 0.55$ and $0.55 < z < 0.85$, respectively (see Table 1 of Carlberg et al. 1997a).

We performed a standard χ^2 fit to the data points in terms of $\log N(> M)$ with three free parameters: Ω_0 , σ_8 and w . Since the data are in the form of a $\log N(> M)$ value per

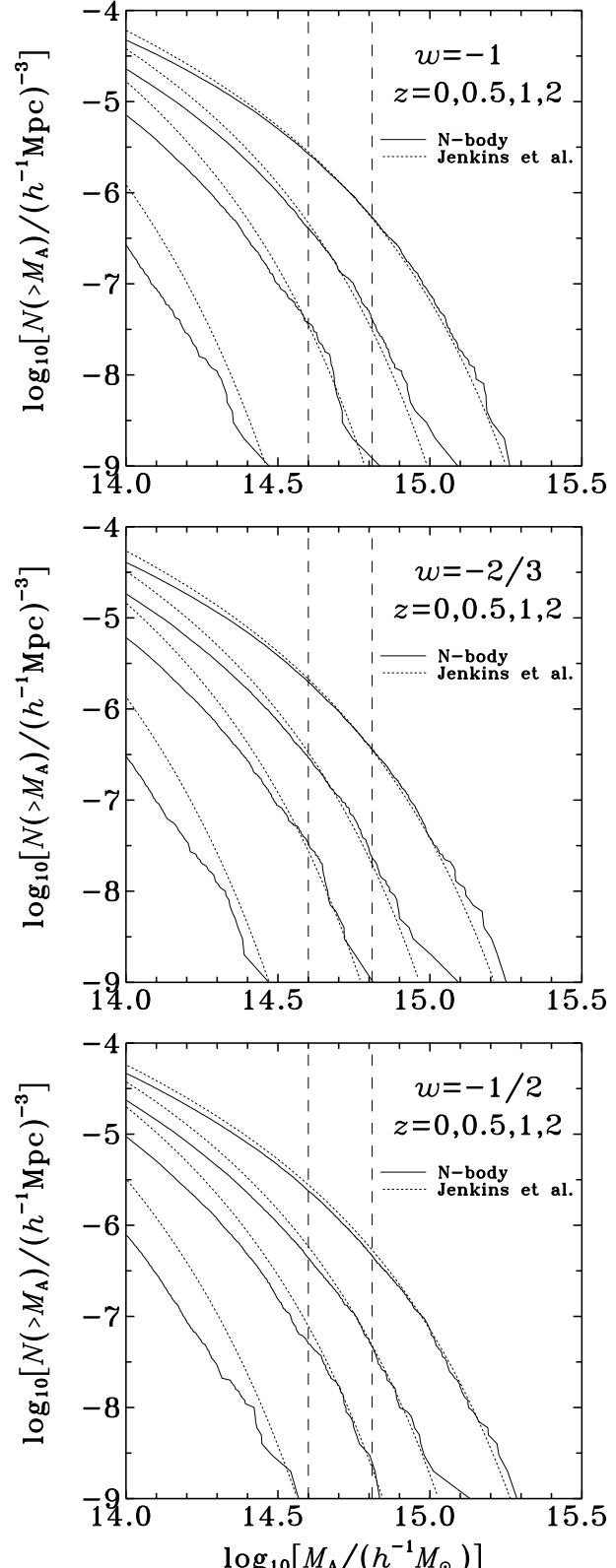


Figure 4. Cumulative mass functions in terms of Abell masses measured in N -body simulations (solid lines) and obtained from the predictions of the Jenkins formula with mass transformation (dotted lines) for $w = -1$, $w = -2/3$ and $w = -1/2$ and at different redshifts. The two vertical dashed lines in each panel indicate the mass range of the data used in Section 5.

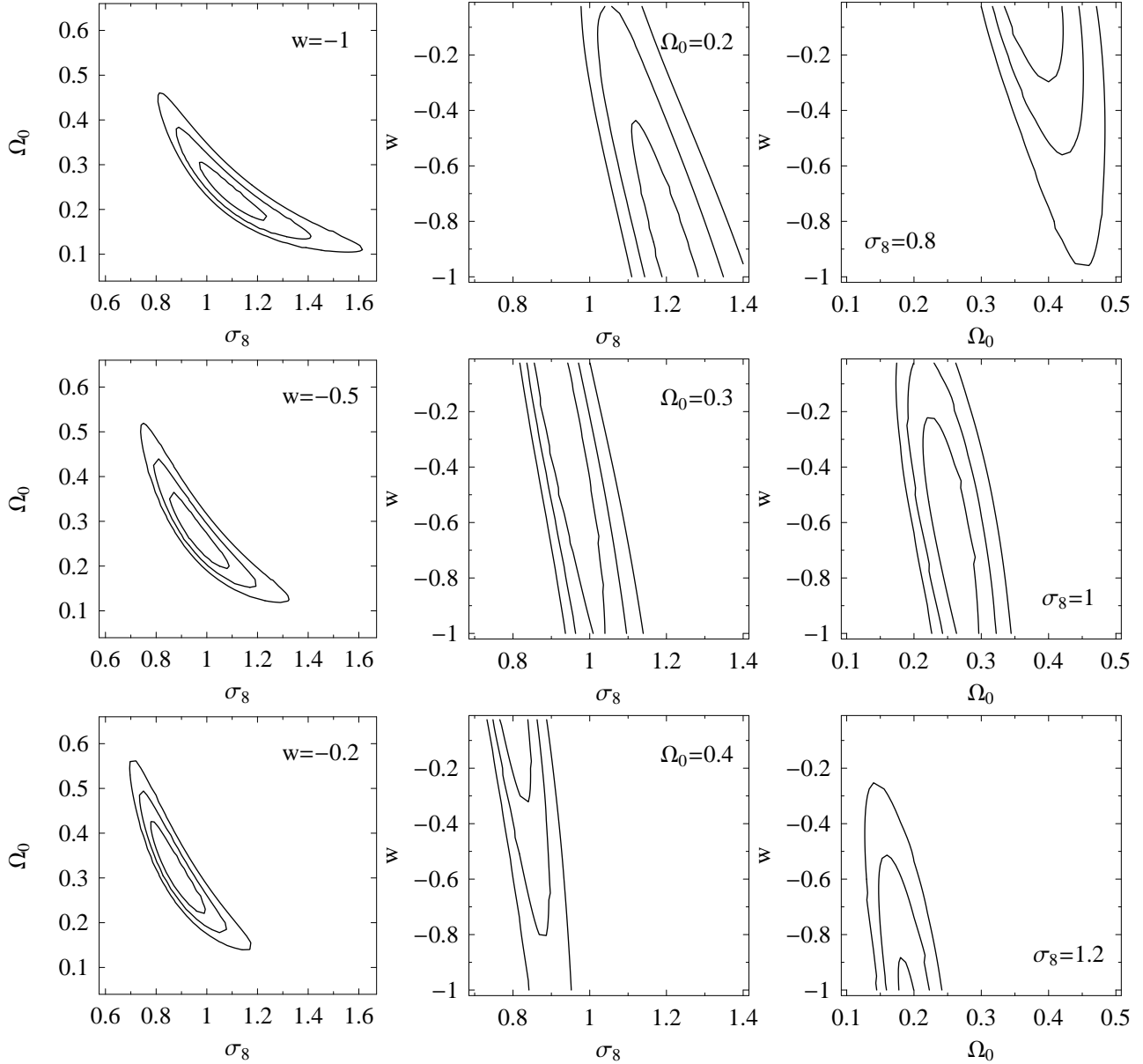


Figure 5. The 1σ , 2σ and 3σ probability contours in the $\sigma_8 - \Omega_0$ (left column), $\sigma_8 - w$ (middle column) and $\Omega_0 - w$ plane (right column) resulting from the fits to the cluster mass function data of Carlberg et al. (1997a). The assumed value of the third parameter is given in the corner of each panel.

redshift bin, for the predictions we take the mean redshift of the bin (it is not necessary to average over redshift because $\log N(> M)$ is approximately linear in redshift). When considering different Ω_0 in models we adjust the data point by linearly interpolating between the data given in Carlberg et al. (1997a) for $\Omega_0 = 0.2$ and $\Omega_0 = 1$. The analysis has been done only for flat models, i.e. we kept $q_0 = 1 - \Omega_0$. We also assumed Hubble constant $h = 0.7$ and the primordial spectral index $n = 1$.

Figure 5 shows the 1σ , 2σ and 3σ probability contours

in the $\sigma_8 - \Omega_0$ (left column), $\sigma_8 - w$ (middle column) and $\Omega_0 - w$ (right column) parameter planes respectively. For each plane the cuts through the confidence region are done for three values of the third parameter; the value is indicated at the corner of each panel. The contours correspond to $\Delta\chi^2 = \chi^2 - \chi^2_{\min} = 3.53, 8.02, 14.2$, where the minimum value $\chi^2_{\min} = 10.1$ is obtained for $\Omega_0 = 0.32$, $\sigma_8 = 0.85$ and $w \rightarrow 0$.

The contours in the $\sigma_8 - \Omega_0$ plane presented in the left column of Figure 5 are the cuts through the confidence

region at (from top to bottom) $w = -1$, $w = -0.5$ and $w = -0.2$. They show a typical shape obtained in this kind of analyses. However, the three cuts through the confidence space shown in this column of Figure 5 actually move significantly when the assumed value of w is changed (note that the axes scales in the left column of the Figure are the same in each panel). Taking into account the dependence on w and the variability of the contours in the whole range $-1 \leq w < 0$, we find $\Omega_0 = 0.32 \pm 0.15$ and $\sigma_8 = 0.85^{+0.38}_{-0.12}$ at 68% confidence level. While for $w = -0.2$ the best-fitting values of the remaining parameters are $\Omega_0 = 0.3$, $\sigma_8 = 0.9$, for lower w the contours move towards lower Ω_0 and higher σ_8 . For $w = -1$ they are centered on $\Omega_0 \approx 0.2$, $\sigma_8 \approx 1.1$.

The middle and right columns of Figure 5 show the constraints on w in two planes, $\sigma_8 - w$ and $\Omega_0 - w$ respectively. The middle column has the cuts for $\Omega_0 = 0.2$, $\Omega_0 = 0.3$ and $\Omega_0 = 0.4$ from the top to the bottom panel, while in the right column the values of the third parameter are $\sigma_8 = 0.8$, 1 and 1.2 . As can be seen in the plots, there is a strong degeneracy between w and any of the two remaining parameters. The particular shape of the contours can be understood by referring back to Figure 1, showing the growth rate of density fluctuations for different w . By changing the normalization of the curves in the Figure to give the same value of $D(a)$ at present ($a = 1$), it is easily seen that the magnitude of density fluctuations drops faster with redshift for more negative w . Thus in order to reproduce a given redshift dependence of the cluster mass function data, for a more negative w and a given Ω_0 (σ_8) a higher value of σ_8 (Ω_0) is needed (as both these parameters enhance the growth of structure).

6 DISCUSSION

The confidence regions we obtained in Figure 5 in the $\sigma_8 - \Omega_0$ plane are qualitatively similar to the results of the analysis of the same data by Carlberg et al. (1997a), which differed from our approach in that they used the Press & Schechter (1974) approximation, a power-law distribution of mass in clusters, and did not consider the dependence on w . While for $w = -0.2$ the best-fitting values of the remaining parameters are $\Omega_0 = 0.3$, $\sigma_8 = 0.9$ in very good agreement with other estimates (e.g. from CMB, see Spergel et al. 2003 or type Ia supernovae, see Tonry et al. 2003), for lower w the contours move towards lower Ω_0 and higher σ_8 . At $w = -1$ they are centered on $\Omega_0 \approx 0.2$, $\sigma_8 \approx 1.1$.

A very similar methodology is provided by using Sunyaev-Zeldovich cluster surveys to probe the evolution of the surface density of clusters as a function of redshift (Battye & Weller 2003 and references therein). The constraints derived by the Sunyaev-Zeldovich surveys are based on the same physical processes and models as those employed here, namely the mass spectrum of haloes in the quintessential cosmology. Battye & Weller (2003) studied the constraining power of Sunyaev-Zeldovich surveys by analyzing mock catalogs of future surveys. Comparing the results obtained here and by Battye & Weller we find that apart from the future PLANCK survey the Carlberg et al. (1997a) data provide tighter or comparable constraints to the Sunyaev-Zeldovich surveys. The PLANCK cluster survey will reduce the uncertainties in σ_8 and Ω_0 by roughly a factor of 2 in comparison with the present results.

Assuming the Λ CDM cosmological model, Bahcall et al. (2003) used data from the SDSS collaboration to estimate that for $\Omega_0 \approx 0.2$, $\sigma_8 \approx 0.9$, a lower value than found here. However, the current result includes higher redshift data, which leads to higher estimates for σ_8 , independent of Ω_0 (Bahcall & Bode 2003). It seems that assuming $w = -1$ when considering cluster abundances leads to rather low values of Ω_0 (or alternatively, high values of σ_8); as pointed out by Oguri et al. (2003), these are in mild conflict with most other estimates. Oguri et al. (2003) suggested that decaying cold dark matter may resolve this discrepancy. Our results offer another possibility: they show that the constraints on Ω_0 and σ_8 from cluster mass functions are in better agreement with other estimates if the assumption of $w = -1$ is relaxed and a less negative value of w is adopted.

We have demonstrated the existence of a strong degeneracy between w and any of the two remaining parameters, Ω_0 and σ_8 , which is not broken in spite of using high redshift data: reproducing the evolution of the cluster mass function data requires a higher value of Ω_0 or σ_8 for more negative w . As discussed by Douspis et al. (2003) and Crooks et al. (2003) the degeneracies between w and other cosmological parameters also plague the constraints obtained from other, e.g. CMB, data sets.

The best fit to the cluster mass function data is obtained for a surprisingly high value of $w \approx 0$, but the dependence on w is rather weak and no value in the entire considered range $-1 \leq w < 0$ can actually be excluded: for every value in this range a reasonable combination of Ω_0 and σ_8 can be found which places the point in 1σ confidence region. It is interesting to note, however, that depending on the values of Ω_0 and σ_8 , we get upper or lower limit on w : for high Ω_0 and low σ_8 the contours tend to provide a lower limit on w , while for low Ω_0 and high σ_8 we have an upper limit. Combined with additional constraints on Ω_0 or σ_8 from other data sets, cluster mass functions can therefore prove useful in estimating the value of w . With the estimates of the cosmological parameters presently available they would provide a lower limit on w . For example, for the best estimates from WMAP (Spergel et al. 2003), $\Omega_0 = 0.27$ and $\sigma_8 = 0.9$, the constraint from our analysis is $-0.5 < w < 0$ at 95% confidence level. At the same confidence level, WMAP in combination with other astronomical data gives $w < -0.78$ (Spergel et al. 2003) while from the SNIa data Tonry et al. (2003) obtain $w < -0.73$. This means that the agreement can be reached only if the estimates are pushed towards their limits or the cosmological model with constant w has to be rejected.

ACKNOWLEDGEMENTS

We thank Ofer Lahav and Gary Mamon for their comments on the manuscript. This work was supported in part by the Polish KBN grant 2P03D02319. Computer time to perform N -body simulations was provided by NCSA. PB received support from NCSA NSF Cooperative Agreement ASC97-40300, PACI Subaward 766. YH acknowledges support from the Israel Science Foundation (143/02) and the Sheinborn Foundation.

REFERENCES

Bahcall N. A., Bode P., 2003, *ApJL*, 588, 1

Bahcall N. A., Fan X., Cen R., 1997, *ApJL*, 485, 53

Bahcall N. A. et al., 2003, *ApJ*, 585, 182

Balbi A., Baccigalupi C., Matarrese S., Perrotta F., Vittorio N., 2001, *ApJL*, 547, 89

Barger V., Marfatia D., 2001, *Phys. Lett. B*, 498, 67

Battye R. A., Weller J., 2003, *Phys. Rev. D*, in press, astro-ph/0305568

Biviano A., Girardi, M., 2003, *ApJ*, 585, 205

Bode P., Ostriker J. P., 2003, *ApJS*, 145, 1

Bode P., Ostriker J.P., Xu G., 2000, *ApJS*, 128, 561

Bode P., Bahcall N. A., Ford E. B., Ostriker J. P., 2001, *ApJ*, 551, 15

Bullock J. S., Kolatt T. S., Sigad Y., Somerville R. S., Kravtsov A. V., Klypin A. A., Primack J. R., Dekel A., 2001, *MNRAS*, 321, 559

Caldwell R. R., Doran M., 2003, astro-ph/0305334

Caldwell R. R., Dave R., Steinhardt P. J., 1998, *Phys. Rev. Lett.*, 80, 1582

Caldwell R. R., Doran M., Müller C. M., Schäfer G., Wetterich C., 2003, *ApJL*, 591, 75

Carlberg R. G., Morris S. L., Yee H. K. C., Ellingson E., 1997a, *ApJ*, 479, L19

Carlberg R. G. et al. 1997b, *ApJ*, 485, L13

Crooks J. L., Dunn J. O., Frampton P. H., Norton H. R., Takanashi T., 2003, astro-ph/0305495

Doran M., Lilley M. J., Schwindt J., Wetterich, C., 2001, *ApJ*, 559, 501

Douspis M., Riazuelo A., Zolnierowski Y., Blanchard A., 2003, *A&A*, 405, 409

Eisenstein D. J., Hut P., 1998, *ApJ*, 498, 462

Harun-or-Rashid S. M., Roos M., 2001, *A&A*, 373, 369

Huterer D., Turner M. S., 2001, *Phys. Rev. D*, 64, 123527

Jenkins A., Frenk C. S., White S. D. M., Colberg J. M., Cole S., Evrard A. E., Couchman H. M. P., Yoshida N., 2001, *MNRAS*, 321, 372

Jimenez R., 2003, *New Astron. Rev.*, in press, astro-ph/0305368

Jing Y. P., 2000, *ApJ*, 535, 30

Jing Y. P., Suto Y., 2000, *ApJL*, 529, 69

Klypin A. A., Maccio A. V., Mainini R., Bonometto S. A., 2003, submitted to *ApJ*, astro-ph/0303304

Krauss L. M., 2003, Proc. ESO-CERN-ESA Symposium on Astronomy, Cosmology and Fundamental Physics, in press, astro-ph/0301012

Linder E. V., Jenkins A., 2003, *MNRAS*, in press, astro-ph/0305286

Lokas E. L., Mamon G. A., 2003, *MNRAS*, 343, 401

Ma C. P., Caldwell R. R., Bode P., Wang L., 1999, *ApJ*, 521, L1

Maor I., Brustein R., Steinhardt P. J., 2001, *Phys. Rev. Lett.* 86, 6

Majumdar S., Mohr J. J., 2003, submitted to *ApJ*, astro-ph/0305341

Navarro J. F., Frenk C. S., White S. D. M., 1997, *ApJ*, 490, 493

Oguri M., Takahashi K., Ohno H., Kotake K., 2003, *ApJL*, in press, astro-ph/0306020

Press W. H., Schechter P., 1974, *ApJ*, 187, 425

Ratra B., Peebles P. J. E., 1988, *Phys. Rev. D*, 37, 3406

Silveira V., Waga I., 1994, *Phys. Rev. D*, 50, 4890

Spergel D. N. et al., 2003, *ApJS*, 148, 175

Steinhardt P. J., Wang L., Zlatev I., 1999, *Phys. Rev. D*, 591, 270

Sugiyama N., 1995, *ApJ*, 471, 542

Tonry J. L. et al., 2003, *ApJ*, in press, astro-ph/0305008

Wang L., Caldwell R. R., Ostriker J. P., Steinhardt P. J., 2000, *ApJ*, 530, 17

Weinberg N. N., Kamionkowski M., 2003, *MNRAS*, 341, 251

Weller J., Albrecht A., 2001, *Phys. Rev. Lett.*, 86, 1939

Zlatev I., Wang L., Steinhardt P. J., 1999, *Phys. Rev. Lett.*, 82, 896